

# Importance of nonlinear long-range electron-phonon interaction on the carrier mobility of anharmonic halide perovskites

Matthew Houtput,<sup>1</sup> Ingvar Zappacosta,<sup>1</sup> Serghei Klimin,<sup>1</sup>  
Samuel Poncé,<sup>2,3</sup> Jacques Tempere,<sup>1</sup> and Cesare Franchini<sup>4,5</sup>

<sup>1</sup>*Theory of Quantum Systems and Complex Systems,  
Universiteit Antwerpen, B-2000 Antwerpen, Belgium*

<sup>2</sup>*European Theoretical Spectroscopy Facility and Institute of Condensed Matter and Nanosciences,  
Université catholique de Louvain, Chemin des Étoiles 8, B-1348 Louvain-la-Neuve, Belgium*

<sup>3</sup>*WEL Research Institute, avenue Pasteur 6, 1300 Wavre, Belgium*

<sup>4</sup>*Faculty of Physics, Computational Materials Physics,  
University of Vienna, Kolingasse 14-16, Vienna A-1090, Austria*

<sup>5</sup>*Department of Physics and Astronomy, Alma Mater Studiorum - Università di Bologna, Bologna, 40127 Italy*

The interaction between the electrons and the lattice vibrations in a solid is responsible for various important effects, such as formation of polarons, temperature dependent bandgaps, phonon-limited carrier transport, and conventional superconductivity. Most works assume a linear electron-phonon interaction, where the electron only interacts with one phonon at a time. However, the validity of this assumption has not been verified in polar anharmonic materials, where large ionic displacements may invalidate the assumption of linear interaction. Here, we show that nonlinear electron-phonon interactions contribute significantly to the finite-temperature electron mobility of the inorganic lead halide perovskite CsPbI<sub>3</sub>. We calculate the electron mobility from first principles using the self-energy relaxation time approximation and the long-range approximation. The effect of nonlinear interaction is taken into account using the recently derived expression for the long-range part of the one-electron-two-phonon matrix element. We show that due to the low phonon frequencies of CsPbI<sub>3</sub>, the one-electron-two-phonon interaction changes the temperature scaling of the mobility and contributes about 10% to the mobility at room temperature. The results underscore the importance of including nonlinear electron-phonon interaction in anharmonic halide perovskites.

Halide perovskites are known for their excellent optoelectronic properties [1–3]. This has led to their usage in the development of several promising technological applications, such as solar cells [4–6] and energy-efficient lighting [7, 8]. A particularly important property in the context of these applications is the charge transport [9], usually quantified by the carrier mobility  $\mu$ . A deeper understanding of the microscopic processes that govern mobility is therefore desirable.

In most materials, this microscopic understanding can be found from the theory of phonon-limited transport [10]. One assumes that the charge carriers can interact with harmonic phonons with frequencies  $\omega_{\mathbf{q}\nu}$ , through a linear electron-phonon scattering process as shown in Fig. 1a. Then, a common way to calculate the carrier mobility  $\mu$  is to calculate the electron energies  $\varepsilon_{\mathbf{k}n}$ , phonon frequencies  $\omega_{\mathbf{q}\nu}$ , and electron-phonon matrix elements  $g_{m\nu}(\mathbf{k}, \mathbf{q})$  from first principles [11], and use these to solve the linearized Boltzmann transport equation for the carrier mobility [10]. However, many of the assumptions in this theory are not applicable to most halide perovskites. For example, it has been shown that several of the halide perovskites are strongly anharmonic [12–16], requiring a treatment with renormalized phonon frequencies and spectral broadening, or even the full phonon spectral function. It has also been suggested that the quasiparticle picture might not be valid in halide perovskites [14], requiring a treatment beyond the Boltzmann transport equation [17]. The violation of these common assumptions makes comparison with experimen-

tal measurements of the mobility [18–23] difficult.

We show here that another common assumption is violated in halide perovskites: the assumption of linear electron-phonon interaction. This approximation is often made out of necessity, as the electron-phonon matrix elements for higher-order electron-phonon interactions such as the one in Fig. 1b are not known. Regardless, it has been predicted that some halide perovskites get significant contributions to the band gap renormalization from nonlinear electron-phonon interaction [24, 25]. A similar prediction has been made for the carrier mobility [25] but only in the adiabatic approximation where the ions are treated classically.

In this Letter, we quantify the effect of the nonlinear one-electron-two-phonon interaction on the carrier mobility of cesium lead iodide (CsPbI<sub>3</sub>), a representative inorganic halide perovskite. There have been several treatments of nonlinear electron-phonon interaction in the literature in recent years [26–34], but most focus on lattice model Hamiltonians [35–51]. We note that nonlinear interaction should not be confused with higher-order treatments of the linear interaction, such as those which include the crossing diagrams [52, 53]. In order to treat the nonlinear interaction from first principles, we use the recently derived expression for the dipole long-range part of the one-electron-two-phonon matrix element  $g_{m\nu_1\nu_2}(\mathbf{k}, \mathbf{q}_1, \mathbf{q}_2)$  [54]. All material properties that enter this matrix element can be calculated from first principles. Since the linear electron-phonon interaction in CsPbI<sub>3</sub> is dominated by the long-range contri-

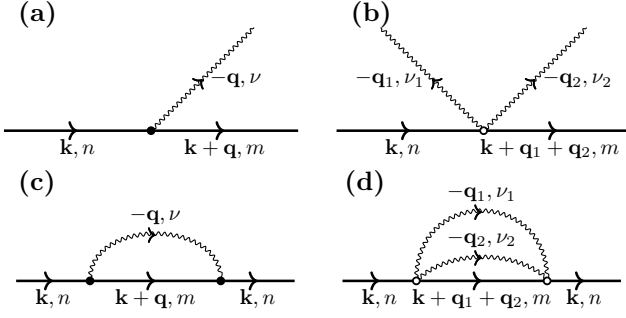


Figure 1. (a)-(b) Feynman diagrams for the linear and lowest-order nonlinear electron-phonon interaction. In (a), the long-range approximation amounts to  $\mathbf{q} \rightarrow \mathbf{0}$ , and in (b) it amounts to  $-\mathbf{q}_1 \rightarrow \mathbf{q}_2$ . (c)-(d) Contributions to the imaginary part of the retarded self energy that are taken into account in this article, where (c) is the Fan-Migdal diagram, and (d) is its nonlinear analog. We do not include the Debye-Waller diagram since it is real.

bution [9, 55, 56], we expect this analysis to be representative for the full nonlinear one-electron-two-phonon interaction in CsPbI<sub>3</sub>.

We investigate the relative contributions of the linear and nonlinear electron-phonon interaction to the carrier mobility in the cubic phase of CsPbI<sub>3</sub>. In order to use the theory derived in Ref. [54], we use the harmonic and quasiparticle approximations. As discussed, these are likely poor approximations in CsPbI<sub>3</sub>. However, since both the linear and nonlinear electron-phonon interaction are treated with the same approximations, this method will still allow to identify whether the nonlinear interaction is negligible or not. Potential directions for a relaxation of these assumptions are discussed at the end of the manuscript.

The drift electron mobility can be computed with the Boltzmann transport equation (BTE) [10]:

$$\mu_{\alpha\beta} = \frac{-e}{n_e(2\pi)^3} \sum_{n \in \text{CB}} \int_{1\text{BZ}} d^3\mathbf{k} v_{\mathbf{k}n\alpha} \partial_{E_\beta} f(\varepsilon_{\mathbf{k}n}). \quad (1)$$

Here  $\alpha, \beta \in \{x, y, z\}$  represent Cartesian directions,  $e$  is the elementary charge,  $n_e$  is the electron density,  $\hbar\mathbf{k}$  is the crystal momentum and is restricted to the first Brillouin zone (1BZ),  $n$  labels the electron bands restricted to the conduction bands,  $\varepsilon_{\mathbf{k}n}$  are the electron band energies, and  $v_{\mathbf{k}n\alpha} = \frac{1}{\hbar} \frac{\partial \varepsilon_{\mathbf{k}n}}{\partial k_\alpha}$  are the band velocities. Finally, the most important quantity that appears in Eq. (1) is the out of equilibrium occupation function  $\partial_{E_\beta} f(\varepsilon_{\mathbf{k}n})$  due to an applied electric field  $E_\beta$  applied in the direction  $\beta$ .

In the self-energy relaxation time approximation (SERTA) [57], the out-of-equilibrium electronic occupation functions reduce to:

$$\partial_{E_\beta} f(\varepsilon_{\mathbf{k}n}) = \frac{\partial f^0(\varepsilon_{\mathbf{k}n})}{\partial \varepsilon_{\mathbf{k}n}} v_{\mathbf{k}n\beta} \tau_{\mathbf{k}n}, \quad (2)$$

Here,  $f^0(\varepsilon)$  is the equilibrium occupation function for the electrons, which is the Fermi-Dirac distribution. Ad-

ditionally,  $\tau_{\mathbf{k}n}^{-1}$  are the scattering rates of the electrons with the phonons [10], which can be obtained from the on-shell retarded diagonal electron self energy  $\Sigma_{\mathbf{k}n}^{\text{R}}$  [10]:

$$\frac{1}{\tau_{\mathbf{k}n}} = -2 \text{Im} [\Sigma_{\mathbf{k}n}^{\text{R}}(\varepsilon_{\mathbf{k}n})] \quad (3)$$

If we were to only use the linear electron-phonon interaction, we would be able to use the standard expression for the Fan-Migdal self energy from Fig. 1c, written in terms of  $\varepsilon_{\mathbf{k}n}$ ,  $\omega_{\mathbf{q}\nu}$ , and  $g_{m\nu}(\mathbf{k}, \mathbf{q})$  [10]. Instead, in order to include the one-electron-two-phonon interaction, we use the long-range theory from Ref. [54], where the imaginary part of the retarded self energy was calculated up to lowest order in the electron-phonon interaction. This gives the Fan-Migdal self energy, Fig. 1c, and a similar term due to the nonlinear electron-phonon interaction in Fig. 1d [54]:

$$\Sigma_{\mathbf{k}n}^{\text{R}}(\varepsilon_{\mathbf{k}n}) = \frac{\hbar e^2}{\varepsilon_0(2\pi)^3} \int_0^{+\infty} d\omega \int_{\mathbb{R}^3} d^3\mathbf{Q} \frac{\mathbf{Q} \cdot \mathcal{P}(\omega) \cdot \mathbf{Q}}{(\mathbf{Q} \cdot \varepsilon^\infty \cdot \mathbf{Q})^2} \times \left[ \frac{1 - f^0(\varepsilon_{\mathbf{k}+\mathbf{Q}n}) + n(\hbar\omega)}{\varepsilon_{\mathbf{k}n} - \varepsilon_{\mathbf{k}+\mathbf{Q}n} - \hbar\omega + i\delta} + \frac{f^0(\varepsilon_{\mathbf{k}+\mathbf{Q}n}) + n(\hbar\omega)}{\varepsilon_{\mathbf{k}n} - \varepsilon_{\mathbf{k}+\mathbf{Q}n} + \hbar\omega + i\delta} \right]. \quad (4)$$

In this expression,  $n(\hbar\omega)$  is the Bose-Einstein distribution for phonons, and  $\mathbf{Q} = \mathbf{q} + \mathbf{G}$  represents a phonon momentum extended to the entire reciprocal space  $\mathbb{R}^3$ : this is equivalent to an integral over  $\mathbf{q} \in 1\text{BZ}$  and a sum over reciprocal lattice vectors  $\mathbf{G}$ . We note that the integral over  $\mathbf{Q}$  should decay quickly and approximately vanish at the boundary of the first Brillouin zone in order for the long-range approximation to be valid, so in practice it is irrelevant whether the integration domain is  $\mathbb{R}^3$  or 1BZ.  $\varepsilon^\infty$  and  $\mathcal{P}(\omega)$  are material-specific  $3 \times 3$  tensors:  $\varepsilon_{ij}^\infty$  is the high-frequency dielectric tensor, and  $\mathcal{P}_{ij}(\omega)$  is a dimensionless spectral function which represents the strength of the long-range electron-phonon interaction. For both tensors, the Cartesian directions  $i$  and  $j$  refer to the direction of a constant electric field  $\mathcal{E}_i$  or  $\mathcal{E}_j$  which is induced by the conduction electrons.

Using the theory from Ref. [54], the electron-phonon spectral function can be calculated as a sum of two contributions. The first contribution is  $\mathcal{T}_{ij}(\omega)$ , which is the contribution from the one-electron-two-phonon interaction. It originates from the diagram in Fig. 1d, and is a continuous spectral function which is defined as [54]:

$$\mathcal{T}_{ij}(\omega) \equiv \frac{e^2}{2\hbar\varepsilon_0(2\pi)^3} \sum_{\nu_1\nu_2} \int_{1\text{BZ}} d^3\mathbf{q} Y_{\nu_1\nu_2i}(\mathbf{q}) Y_{\nu_1\nu_2j}^*(\mathbf{q}) \times \left\{ [1 + n(\hbar\omega_{\mathbf{q}\nu_1}) + n(\hbar\omega_{\mathbf{q}\nu_2})] \delta(\omega - |\omega_{\mathbf{q}\nu_1} + \omega_{\mathbf{q}\nu_2}|) + |n(\hbar\omega_{\mathbf{q}\nu_2}) - n(\hbar\omega_{\mathbf{q}\nu_1})| \delta(\omega - |\omega_{\mathbf{q}\nu_1} - \omega_{\mathbf{q}\nu_2}|) \right\}. \quad (5)$$

In this expression,  $Y_{\nu_1\nu_2i}(\mathbf{q})$  serves the same purpose as the mode polarity, in the sense that it represents the

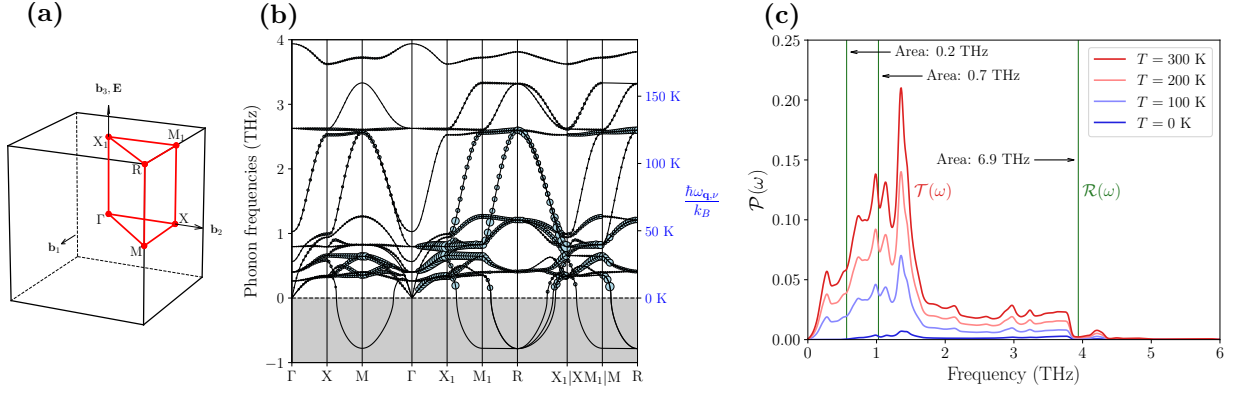


Figure 2. First principles results for the nonlinear electron-phonon properties of CsPbI<sub>3</sub> in the cubic phase. **(a)** High-symmetry Brillouin zone path for a simple cubic material, with an electric field breaking the symmetry in the  $z$ -direction. **(b)** Phonon frequencies  $\omega_{\mathbf{q}\nu}$  of cubic CsPbI<sub>3</sub> at zero temperature. The overlaid circles have areas proportional to  $\sum_{\nu'} |Y_{\nu\nu',z}(\mathbf{q})|^2$ , i.e. the magnitude of the long-range interaction strengths between the phonon ( $\mathbf{q}\nu$ ) and all other phonons of the form ( $-\mathbf{q}\nu'$ ). There are imaginary phonon modes because the cubic phase is unstable at zero temperature: we set  $Y_{\nu\nu',z}(\mathbf{q}) = 0$  for any branches with  $\omega_{\mathbf{q},\nu} < 0.1$  THz. **(c)** One-electron-two-phonon spectral function  $\mathcal{T}(\omega)$  calculated from Eq. (5) and the data from **(b)**.  $\mathcal{R}(\omega)$  is shown as a sequence of vertical lines representing the Dirac delta functions, with the areas under the delta functions indicated for reference. The effect of the one-electron-two-phonon interaction is significantly enhanced at finite temperatures: this is ultimately due to the very low phonon frequencies of CsPbI<sub>3</sub> (see main text).

strength of the long-range interaction between an electron and two phonons, in branches  $\nu_1, \nu_2$  and with approximately opposite momenta  $-\mathbf{q}_1 \approx \mathbf{q}_2 = \mathbf{q}$ . It is given in terms of the phonon frequencies  $\omega_{\mathbf{q}\nu}$  and eigenvectors  $e_{\kappa\alpha\nu}(\mathbf{q})$ , and the derivative of the dynamical matrix with respect to the induced electric field  $\frac{\partial \mathcal{D}_{\kappa\alpha,\kappa'\beta}(\mathbf{q})}{\partial \mathcal{E}_i}$  [54]:

$$Y_{\nu_1\nu_2 i}(\mathbf{q}) \equiv \frac{1}{ie} \sqrt{\frac{\hbar}{2\omega_{\mathbf{q}\nu_1}} \frac{\hbar}{2\omega_{\mathbf{q}\nu_2}}} \times \sum_{\kappa\alpha\kappa'\beta} e_{\kappa\alpha\nu_1}^*(\mathbf{q}) \frac{\partial \mathcal{D}_{\kappa\alpha,\kappa'\beta}(\mathbf{q})}{\partial \mathcal{E}_i} e_{\kappa'\beta\nu_2}(\mathbf{q}). \quad (6)$$

In this manuscript, we focus on the cubic phase of CsPbI<sub>3</sub>. In this case,  $\varepsilon^\infty$ ,  $\mathcal{P}(\omega)$ , and  $\mathcal{T}(\omega)$  all reduce to scalars [54]:

$$\varepsilon_{ij}^\infty = \varepsilon^\infty \delta_{ij}, \quad (7)$$

$$\mathcal{P}_{ij}(\omega) = \mathcal{P}(\omega) \delta_{ij}, \quad (8)$$

$$\mathcal{T}_{ij}(\omega) = \mathcal{T}(\omega) \delta_{ij}. \quad (9)$$

Since these tensors only have a single independent component, it is sufficient to align the electric field  $\mathcal{E}$  along only one of the three cartesian axes. In this manuscript, we arbitrarily choose  $\mathcal{E}$  along the  $z$ -direction, meaning that we calculate  $\mathcal{T}(\omega) \equiv \mathcal{T}_{zz}(\omega)$  by setting  $i = j = z$  in Eq. (5).

The second contribution is  $\mathcal{R}(\omega)$ , which is the Fröhlich-type contribution from the linear electron-phonon interaction [58–60]. It is a sum of delta functions at the longitudinal optical phonon frequencies  $\omega_\nu$  at  $\mathbf{q} = \mathbf{0}$  [54]:

$$\mathcal{R}(\omega) \equiv \frac{e^2}{2\varepsilon_0\Omega_0} \sum_\nu \frac{|p_\nu|^2}{\omega_\nu} \delta(\omega - \omega_\nu), \quad (10)$$

where  $\Omega_0$  is the size of the unit cell and  $p_\nu$  is the mode polarity, which represents the strength of the long-range interaction between an electron and one phonon branch  $\nu$  with momentum  $\mathbf{q} \approx \mathbf{0}$  [54]. Once both contributions are known,  $\mathcal{P}(\omega)$  is simply evaluated as the sum of the two:

$$\mathcal{P}(\omega) = \mathcal{R}(\omega) + \mathcal{T}(\omega). \quad (11)$$

We note that  $\mathbf{q}$  is not restricted to  $\mathbf{q} \approx \mathbf{0}$  Eqs. (5)-(6). Therefore, to calculate the nonlinear spectral function  $\mathcal{T}(\omega)$  using Eq. (5), we need the phonon frequencies over the entire first BZ, despite making the long-range approximation [54]. This is counterintuitive because for the familiar linear electron-phonon interaction, only phonons with  $\mathbf{q} \approx \mathbf{0}$  contribute to Eq. (10).

The  $p_\nu$  in Eq. (10) can be written in terms of the Born effective charge tensor and phonon eigenvectors, and  $Y_{\nu_1\nu_2 z}(\mathbf{q})$  can be written in terms of phonon frequencies and eigenvectors as well as their derivative with respect to an external electric field [54]. All of these can be calculated from first principles (see Sec. S2 in the Supplemental Material [61] and references [62–67] therein), which allows to evaluate the self energy in Eq. (4). Finally, in order to compute the electron mobility in Eq. (1), we need an expression for the electron bands  $\varepsilon_{\mathbf{k}n}$ . At sufficiently low carrier densities, only the electronic states close to the conduction band will contribute. Around the conduction band minimum, CsPbI<sub>3</sub> has a single parabolic conduction band, which we label with  $n = c$ :

$$\varepsilon_{\mathbf{k}c} = \frac{\hbar^2 |\mathbf{k}|^2}{2m_c^*}, \quad (12)$$

where we take  $m_c^* = 0.17m_e$  for the effective band mass of the electron [9]. We note that at low carrier densities,

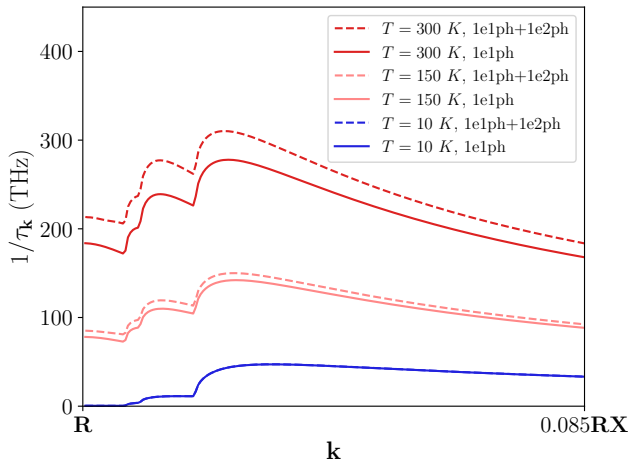


Figure 3. Inverse electron lifetimes in cubic CsPbI<sub>3</sub>, close to the conduction band minimum at the  $\mathbf{R}$ -point, calculated using Eqs. (3)-(4) and the first-principles data of Fig. 2. Full lines are calculated using only the linear electron-phonon interaction from Eq. (10), while dashed lines also include the nonlinear interaction from Eq. (5). The nonlinear interaction is negligible at low temperatures but contributes more at room temperature.

the hole mobility in Eq. (1) is the same as for the electrons, except that we need to use the effective hole mass  $m_v^* = 0.16m_e$  [9]. Ultimately, the effective band mass  $m^*$  only enters the mobility as a prefactor according to  $\mu \sim (m^*)^{-\frac{3}{2}}$  (see also Eq. (S30) in the Supplemental Material [61]): it does not affect the relative contributions of the linear and nonlinear electron-phonon interaction. All presented results will be for the electron mobility, since the relative effects constitute the main result we are interested in.

Fig. 2 shows the material properties of cubic CsPbI<sub>3</sub> needed for the retarded self energy in Eq. (4), calculated from first principles using the method described in Ref. [54]. These material properties include the phonon frequencies  $\omega_{\mathbf{q}\nu}$ , the one-electron-two-phonon strengths  $Y_{\nu_1\nu_2z}(\mathbf{q})$ , and the electron-phonon spectral function  $\mathcal{P}(\omega) = \mathcal{R}(\omega) + \mathcal{T}(\omega)$ . Additionally, we have calculated  $\varepsilon^\infty = 5.96$  for the dielectric tensor of CsPbI<sub>3</sub>, close to other first principles calculations in the literature [9, 68]. Fig. 2b confirms that  $Y_{\nu_1\nu_2z}(\mathbf{q})$  gets nonzero contributions from all over the Brillouin zone, indicating that the continuum approximation would not be applicable here. The phonon calculations, with and without external electric field, were all performed in the harmonic approximation at zero temperature. This means that there are imaginary phonon modes in Fig. 2, since the cubic phase is only stabilized by anharmonic effects at finite temperatures [69]. At lower temperatures, the tetragonal or orthorhombic phases are stable. However, due to the computational cost of a larger unit cell with an external electric field, we are limited to the cubic phase. To calculate the nonlinear electron-phonon spectral func-

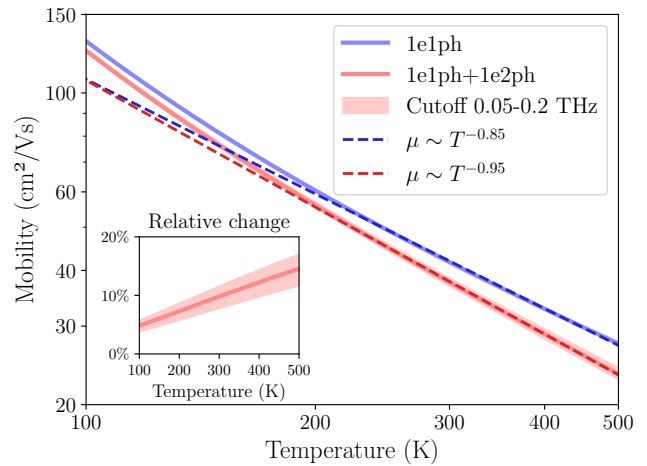


Figure 4. SERTA mobility of CsPbI<sub>3</sub> as a function of temperature, calculated using Eq. (1) and the electron lifetimes of Fig. 3. The solid blue line is calculated using only the linear electron-phonon interaction from Eq. (10), and the solid red line is calculated including the one-electron-two-phonon interaction from Eq. (5). Both are calculated using a frequency cutoff of 0.1 THz; the red shaded area shows the result when this cutoff is varied between 0.05 THz and 0.2 THz, indicating that the nonlinear contribution remains significant regardless of this cutoff value. Dashed lines indicate power law fits in the region between 200 – 500 K. The inset shows the relative change of the mobility due to the one-electron-two-phonon interaction, relative to the mobility when nonlinear interaction is neglected.

tion  $\mathcal{T}(\omega)$  in Fig. 2c, we set  $Y_{\nu_1\nu_2z}(\mathbf{q}) = 0$  for all branches with frequencies  $\omega_{\mathbf{q}\nu} < 0.1$  THz in order to circumvent the imaginary branches. The value 0.1 THz is arbitrarily chosen; later, we show results with the cutoff varying from 0.05 THz to 0.2 THz to show that the qualitative conclusions are independent of this choice. It is unclear exactly how much the imaginary modes would contribute to the nonlinear electron-phonon spectral function  $\mathcal{T}(\omega)$ , if they were included using an anharmonic phonon theory. However, one can see from Eq. (5) that all branches provide positive contributions to  $\mathcal{T}(\omega)$ , so it stands to reason that the results presented here represent an underestimation of the effect of nonlinear electron-phonon interaction.

Importantly, the linear electron-phonon spectral function  $\mathcal{R}(\omega)$  is independent of temperature, whereas the nonlinear electron-phonon spectral function  $\mathcal{T}(\omega)$  depends on temperature through the Bose-Einstein distributions  $n(\hbar\omega_{\mathbf{q}\nu})$ . At sufficiently large temperatures  $k_B T \gg \hbar\omega_{\mathbf{q}\nu}$ , the Bose-Einstein distribution satisfies  $n(\hbar\omega_{\mathbf{q}\nu}) \approx \frac{k_B T}{\hbar\omega_{\mathbf{q}\nu}} - \frac{1}{2}$  so that Eq. (5) scales linearly with temperature. CsPbI<sub>3</sub> has low phonon frequencies, so all phonons are thermally activated at room temperature. Additionally, Fig. 2b shows that most of the contributions to  $\mathcal{T}(\omega)$  come from phonons with frequencies lower than 1 THz. Therefore, we see a strong temper-

ature dependence in Fig. 2c. Although  $\mathcal{T}(\omega)$  is very small at zero temperature, it is of order 0.1 at room temperature, which means one needs to look at finite temperature properties of CsPbI<sub>3</sub> in order to see the effect of nonlinear interaction. A similar result is seen for the temperature-dependent bandgap renormalization in methylammonium lead iodide [24].

With the electron-phonon spectral function  $\mathcal{P}(\omega)$  from Fig. 2, we can calculate the electron lifetimes and the SERTA electron mobility (see also Sec. S1 in the Supplemental Material [61] and references [70, 71] therein). These are shown in Fig. 3 and Fig. 4, respectively. In line with the results of Fig. 2, the effects of nonlinear electron-phonon interaction are only revealed at higher temperatures. Above room temperature, the electron mobility in CsPbI<sub>3</sub> is reduced by about 10% by the long-range one-electron-two-phonon interaction. Additionally, the temperature dependence of  $\mathcal{T}(\omega)$  in Fig. 2c changes the temperature scaling of the mobility. In the region between 200 – 500 K, the mobility is described by a power law fit  $\mu \sim T^{-\gamma}$ , but the nonlinear electron-phonon interaction increases the exponent from  $\gamma = 0.85$  to  $\gamma = 0.95$ . The change in the power law exponent is particularly interesting because this is the quantity most often compared to experimental measurements [14, 18, 20, 21, 72]. The present work shows that including the nonlinear electron-phonon interaction measurably increases the power law exponent, which must be taken into account when comparing first-principles and experimental results.

The present work suggests many perspectives for further research, several of which consist of improving the approximations made in this Letter. These perspectives can be separated into two distinct categories: improving the calculation of  $\mathcal{P}(\omega)$ , and using a more refined theory for electronic transport. Firstly, the calculation of  $\mathcal{P}(\omega)$  can be improved by including phonon anharmonicity and all orders of one-electron- $n$ -phonon interactions. Most notably, the results in Figs. 2-4 are based on the harmonic approximation for the phonons, but CsPbI<sub>3</sub> is known to exhibit strong phonon anharmonicity [69]. It is expected that the higher-order nonlinear interactions scale even faster with temperature than the linear and one-electron-two-phonon interaction. Indeed, the lowest order contribution of the one-electron- $n$ -phonon interaction to the self energy contains  $n$  phonon lines. An analogous reasoning as the one performed for the one-electron-two-phonon interaction shows that the one-electron- $n$ -phonon contribution to  $\mathcal{P}(\omega)$  scales as  $T^{n-1}$  at high temperatures. Depending on the prefactors associated with each of these terms, this scaling may significantly affect

the power law scaling of electron mobility at room temperatures, similarly to the result that Fig. 4 shows for the one-electron-two-phonon interaction.

The second category of perspectives is to take any result for the long-range electron-phonon spectral function  $\mathcal{P}(\omega)$  as given, and use it to calculate the electron mobility with more advanced transport theories. One may start from the self energy in Eq. (4), written in terms of  $\mathcal{P}(\omega)$  and the harmonic quantities  $\varepsilon_{\mathbf{k}n}$  and  $\varepsilon^\infty$ . This expression can be used instead of the Fan-Migdal self energy to derive the equivalent Boltzmann transport equation [10], or even more general transport theories that do not make the quasiparticle approximation [17, 73]. This may significantly affect the results for the mobility, even given the same spectral function  $\mathcal{P}(\omega)$ .

We have shown that carrier mobility in CsPbI<sub>3</sub> gains a significant contribution from nonlinear one-electron-two-phonon interaction, which is usually neglected in the literature. The microscopic reason that the nonlinear interaction is non-negligible, is that CsPbI<sub>3</sub> has very low phonon frequencies and therefore large thermal ionic displacements. Therefore, the results may be transferable to other halide perovskites, and perhaps to other soft polar anharmonic materials. The results of this Letter suggest the necessity of further theoretical developments for nonlinear electron-phonon interaction in the halide perovskites, in order to include e.g. anharmonicity, higher-order nonlinear terms, and/or short-range coupling. The theory presented here and in Ref. [54] represents a first step in this promising direction.

#### DATA AVAILABILITY STATEMENT

The first-principles data and postprocessing code used to generate Figs. 2-4 are publicly available online [74].

#### ACKNOWLEDGMENTS

M.H., I.Z., S.K. and J.T. acknowledge the Research Foundation Flanders (FWO), file numbers 1224724N, V472923N, 1120825N, G060820N, G0A9F25N, and G0AIY25N, for their funding of this research. C.F. and J.T. acknowledge support from the joint Austrian Science Fund (FWF) - FWO project I 4506. S. P. is a Research Associate of the Fonds de la Recherche Scientifique - FNRS. This publication was supported by the Walloon Region in the strategic axe FRFS-WEL-T.

[1] D. M. Jang, K. Park, D. H. Kim, J. Park, F. Shojaei, H. S. Kang, J.-P. Ahn, J. W. Lee, and J. K. Song, Reversible Halide Exchange Reaction of Organometal Trihalide Perovskite Colloidal Nanocrystals for Full-Range Band Gap Tuning, *Nano Letters* **15**, 5191 (2015).

[2] S. D. Stranks and H. J. Snaith, Metal-halide perovskites for photovoltaic and light-emitting devices, *Nature Nanotechnology* **10**, 391 (2015).

[3] T. M. Brenner, D. A. Egger, L. Kronik, G. Hodes, and D. Cahen, Hybrid organic-inorganic perovskites: Low-

- cost semiconductors with intriguing charge-transport properties, *Nature Reviews Materials* **1**, 15007 (2016).
- [4] A. Kojima, K. Teshima, Y. Shirai, and T. Miyasaka, Organometal Halide Perovskites as Visible-Light Sensitizers for Photovoltaic Cells, *Journal of the American Chemical Society* **131**, 6050 (2009).
  - [5] M. A. Green, A. Ho-Baillie, and H. J. Snaith, The emergence of perovskite solar cells, *Nature Photonics* **8**, 506 (2014).
  - [6] H. Min, D. Y. Lee, J. Kim, G. Kim, K. S. Lee, J. Kim, M. J. Paik, Y. K. Kim, K. S. Kim, M. G. Kim, T. J. Shin, and S. Il Seok, Perovskite solar cells with atomically coherent interlayers on SnO<sub>2</sub> electrodes, *Nature* **598**, 444 (2021).
  - [7] Z.-K. Tan, R. S. Moghaddam, M. L. Lai, P. Docampo, R. Higler, F. Deschler, M. Price, A. Sadhanala, L. M. Pazos, D. Credgington, F. Hanusch, T. Bein, H. J. Snaith, and R. H. Friend, Bright light-emitting diodes based on organometal halide perovskite, *Nature Nanotechnology* **9**, 687 (2014).
  - [8] X.-K. Liu, W. Xu, S. Bai, Y. Jin, J. Wang, R. H. Friend, and F. Gao, Metal halide perovskites for light-emitting diodes, *Nature Materials* **20**, 10 (2021).
  - [9] S. Ponc e, M. Schlipf, and F. Giustino, Origin of Low Carrier Mobilities in Halide Perovskites, *ACS Energy Letters* **4**, 456 (2019).
  - [10] S. Ponc e, W. Li, S. Reichardt, and F. Giustino, First-principles calculations of charge carrier mobility and conductivity in bulk semiconductors and two-dimensional materials, *Reports on Progress in Physics* **83**, 036501 (2020).
  - [11] F. Giustino, Electron-phonon interactions from first principles, *Reviews of Modern Physics* **89**, 015003 (2017).
  - [12] O. Yaffe, Local Polar Fluctuations in Lead Halide Perovskite Crystals, *Physical Review Letters* **118**, 10.1103/PhysRevLett.118.136001 (2017).
  - [13] A. Gold-Parker, P. M. Gehring, J. M. Skelton, I. C. Smith, D. Parshall, J. M. Frost, H. I. Karunadasa, A. Walsh, and M. F. Toney, Acoustic phonon lifetimes limit thermal transport in methylammonium lead iodide, *Proceedings of the National Academy of Sciences* **115**, 11905 (2018).
  - [14] M. J. Schilcher, P. J. Robinson, D. J. Abramovitch, L. Z. Tan, A. M. Rappe, D. R. Reichman, and D. A. Egger, The Significance of Polarons and Dynamic Disorder in Halide Perovskites, *ACS Energy Letters* **6**, 2162 (2021).
  - [15] X. Zhu and D. A. Egger, Effect of Overdamped Phonons on the Fundamental Band Gap of Perovskites, *Physical Review Letters* **134**, 016403 (2025).
  - [16] J. Yin, O. Hellman, and S. Ponc e, Impact of anharmonicity on the carrier mobility of the Pb-free CsSnBr<sub>3</sub> perovskite (2025), [arXiv:2505.20092 \[cond-mat\]](https://arxiv.org/abs/2505.20092).
  - [17] J.-M. Lihm and S. Ponc e, Beyond-Quasiparticle Transport with Vertex Correction: Self-Consistent Ladder Formalism for Electron-Phonon Interactions, *Physical Review X* **16**, 011008 (2026).
  - [18] H. T. Yi, X. Wu, X. Zhu, and V. Podzorov, Intrinsic Charge Transport across Phase Transitions in Hybrid Organo-Inorganic Perovskites, *Advanced Materials* **28**, 6509 (2016).
  - [19] S. Dastidar, S. Li, S. Y. Smolin, J. B. Baxter, and A. T. Fafarman, Slow Electron-Hole Recombination in Lead Iodide Perovskites Does Not Require a Molecular Dipole, *ACS Energy Letters* **2**, 2239 (2017).
  - [20] S. Shrestha, G. J. Matt, A. Osvet, D. Niesner, R. Hock, and C. J. Brabec, Assessing Temperature Dependence of Drift Mobility in Methylammonium Lead Iodide Perovskite Single Crystals, *The Journal of Physical Chemistry C* **122**, 5935 (2018).
  - [21] A. Biewald, N. Giesbrecht, T. Bein, P. Docampo, A. Hartschuh, and R. Ciesielski, Temperature-Dependent Ambipolar Charge Carrier Mobility in Large-Crystal Hybrid Halide Perovskite Thin Films, *ACS Applied Materials & Interfaces* **11**, 20838 (2019).
  - [22] S. Sarkar, S. Banerjee, A. Swarnkar, and P. Mandal, Effect of Capping Ligand Engineering on Transport Properties and Carrier Dynamics in Cubic CsPbI<sub>3</sub> Nanocrystal Film, *The Journal of Physical Chemistry C* **125**, 10539 (2021).
  - [23] Y. J. Lee, J. S. Han, D. E. Lee, T. H. Lee, J. Y. Kim, J. M. Suh, J. H. Lee, I. H. Im, S. J. Kim, K. J. Kwak, and H. W. Jang, High Hole Mobility Inorganic Halide Perovskite Field-Effect Transistors with Enhanced Phase Stability and Interfacial Defect Tolerance, *Advanced Electronic Materials* **8**, 2100624 (2022).
  - [24] W. A. Saidi, S. Ponc e, and B. Monserrat, Temperature Dependence of the Energy Levels of Methylammonium Lead Iodide Perovskite from First-Principles, *The Journal of Physical Chemistry Letters* **7**, 5247 (2016).
  - [25] M. Z. Mayers, L. Z. Tan, D. A. Egger, A. M. Rappe, and D. R. Reichman, How Lattice and Charge Fluctuations Control Carrier Dynamics in Halide Perovskites, *Nano Letters* **18**, 8041 (2018).
  - [26] K. L. Ngai, Two-Phonon Deformation Potential and Superconductivity in Degenerate Semiconductors, *Physical Review Letters* **32**, 215 (1974).
  - [27] Yu. N. Epifanov, A. P. Levanyuk, and G. M. Levanyuk, Interaction of carriers with to-phonons and electrical conductivity of ferroelectrics, *Ferroelectrics* **35**, 199 (1981).
  - [28] D. Van Der Marel, F. Barantani, and C. W. Rischau, Possible mechanism for superconductivity in doped SrTiO<sub>3</sub>, *Physical Review Research* **1**, 013003 (2019).
  - [29] D. E. Kiselov and M. V. Feigel'man, Theory of superconductivity due to Ngai's mechanism in lightly doped SrTiO<sub>3</sub>, *Physical Review B* **104**, L220506 (2021).
  - [30] A. Kumar, V. I. Yudson, and D. L. Maslov, Quasiparticle and Nonquasiparticle Transport in Doped Quantum Paraelectrics, *Physical Review Letters* **126**, 076601 (2021).
  - [31] Kh. G. Nazaryan and M. V. Feigel'man, Conductivity and thermoelectric coefficients of doped SrTiO<sub>3</sub> at high temperatures, *Physical Review B* **104**, 115201 (2021).
  - [32] R. Bianco and I. Errea, Non-perturbative theory of the electron-phonon coupling and its first-principles implementation (2023), [arXiv:2303.02621 \[cond-mat\]](https://arxiv.org/abs/2303.02621).
  - [33] T. Yildirim, O. G ulseren, J. W. Lynn, C. M. Brown, T. J. Udovic, Q. Huang, N. Rogado, K. A. Regan, M. A. Hayward, J. S. Slusky, T. He, M. K. Haas, P. Khalifah, K. Inumaru, and R. J. Cava, Giant Anharmonicity and Nonlinear Electron-Phonon Coupling in MgB<sub>2</sub>: A Combined First-Principles Calculation and Neutron Scattering Study, *Physical Review Letters* **87**, 037001 (2001).
  - [34] A. Y. Liu, I. I. Mazin, and J. Kortus, Beyond Eliashberg Superconductivity in MgB<sub>2</sub>: Anharmonicity, Two-Phonon Scattering, and Multiple Gaps, *Physical Review Letters* **87**, 087005 (2001).
  - [35] P. S. Riseborough, The small polaron with nonlinear electron-phonon interactions, *Annals of Physics* **153**, 1

- (1984).
- [36] C. P. J. Adolphs and M. Berciu, Going beyond the linear approximation in describing electron-phonon coupling: Relevance for the Holstein model, *EPL (Europhysics Letters)* **102**, 47003 (2013).
- [37] C. P. J. Adolphs and M. Berciu, Single-polaron properties for double-well electron-phonon coupling, *Physical Review B* **89**, 035122 (2014).
- [38] S. Li and S. Johnston, The effects of non-linear electron-phonon interactions on superconductivity and charge-density-wave correlations, *EPL (Europhysics Letters)* **109**, 27007 (2015).
- [39] S. Li, E. A. Nowadnick, and S. Johnston, Quasiparticle properties of the nonlinear Holstein model at finite doping and temperature, *Physical Review B* **92**, 064301 (2015).
- [40] D. M. Kennes, E. Y. Wilner, D. R. Reichman, and A. J. Millis, Transient superconductivity from electronic squeezing of optically pumped phonons, *Nature Physics* **13**, 479 (2017).
- [41] M. A. Sentef, Light-enhanced electron-phonon coupling from nonlinear electron-phonon coupling, *Physical Review B* **95**, 205111 (2017).
- [42] P. M. Dee, J. Coulter, K. G. Kleiner, and S. Johnston, Relative importance of nonlinear electron-phonon coupling and vertex corrections in the Holstein model, *Communications Physics* **3**, 145 (2020).
- [43] F. Grandi, J. Li, and M. Eckstein, Ultrafast Mott transition driven by nonlinear electron-phonon interaction, *Physical Review B* **103**, L041110 (2021).
- [44] J. Sous, B. Kloss, D. M. Kennes, D. R. Reichman, and A. J. Millis, Phonon-induced disorder in dynamics of optically pumped metals from nonlinear electron-phonon coupling, *Nature Communications* **12**, 5803 (2021).
- [45] N. V. Prokof'ev and B. V. Svistunov, Phonon modulated hopping polarons: X-representation technique, *Physical Review B* **106**, L041117 (2022).
- [46] S. Ragni, T. Hahn, Z. Zhang, N. Prokof'ev, A. Kuklov, S. Klimin, M. Houtput, B. Svistunov, J. Tempere, N. Nagaosa, C. Franchini, and A. S. Mishchenko, Polaron with quadratic electron-phonon interaction, *Physical Review B* **107**, L121109 (2023).
- [47] Z. Zhang, A. Kuklov, N. Prokof'ev, and B. Svistunov, Soliton states from quadratic electron-phonon interaction, *Physical Review B* **108**, 245127 (2023).
- [48] Z. Han, S. A. Kivelson, and P. A. Volkov, Quantum Bipolaron Superconductivity from Quadratic Electron-Phonon Coupling, *Physical Review Letters* **132**, 226001 (2024).
- [49] K. Kovač, D. Golež, M. Mierzejewski, and J. Bonča, Optical Manipulation of Bipolarons in a System with Nonlinear Electron-Phonon Coupling, *Physical Review Letters* **132**, 106001 (2024).
- [50] S. N. Klimin, J. Tempere, M. Houtput, S. Ragni, T. Hahn, C. Franchini, and A. S. Mishchenko, Analytic method for quadratic polarons in nonparabolic bands, *Physical Review B* **110**, 075107 (2024).
- [51] S. Ragni, T. Miškić, T. Hahn, N. Prokof'ev, O. S. Barišić, N. Nagaosa, C. Franchini, and A. S. Mishchenko, Polarons with arbitrary nonlinear electron-phonon interaction, *Physical Review Research* **7**, 043304 (2025).
- [52] M. A. Smondyrev, Diagrams in the polaron model, *Theoretical and Mathematical Physics* **68**, 653 (1986).
- [53] N.-E. Lee, J.-J. Zhou, H.-Y. Chen, and M. Bernardi, Ab initio electron-two-phonon scattering in GaAs from next-to-leading order perturbation theory, *Nature Communications* **11**, 1607 (2020).
- [54] M. Houtput, L. Ranalli, C. Verdi, S. Klimin, S. Ragni, C. Franchini, and J. Tempere, First-principles theory of nonlinear long-range electron-phonon interaction, *Physical Review B* **111**, 184320 (2025).
- [55] C. Q. Xia, J. Peng, S. Poncé, J. B. Patel, A. D. Wright, T. W. Crothers, M. Uller Rothmann, J. Borchert, R. L. Milot, H. Kraus, Q. Lin, F. Giustino, L. M. Herz, and M. B. Johnston, Limits to Electrical Mobility in Lead-Halide Perovskite Semiconductors, *The Journal of Physical Chemistry Letters* **12**, 3607 (2021).
- [56] Y. Yamada and Y. Kanemitsu, Electron-phonon interactions in halide perovskites, *NPG Asia Materials* **14**, 48 (2022).
- [57] S. Poncé, E. R. Margine, and F. Giustino, Towards predictive many-body calculations of phonon-limited carrier mobilities in semiconductors, *Physical Review B* **97**, 121201 (2018).
- [58] H. Fröhlich, Electrons in lattice fields, *Advances in Physics* **3**, 325 (1954).
- [59] A. Miglio, V. Brousseau-Couture, E. Godbout, G. Antonius, Y.-H. Chan, S. G. Louie, M. Côté, M. Giantomassi, and X. Gonze, Predominance of non-adiabatic effects in zero-point renormalization of the electronic band gap, *npj Computational Materials* **6**, 167 (2020).
- [60] B. Guster, P. Melo, B. A. A. Martin, V. Brousseau-Couture, J. C. De Abreu, A. Miglio, M. Giantomassi, M. Côté, J. M. Frost, M. J. Verstraete, and X. Gonze, Fröhlich polaron effective mass and localization length in cubic materials: Degenerate and anisotropic electronic bands, *Physical Review B* **104**, 235123 (2021).
- [61] See Supplemental Material for further derivations and numerical parameters.
- [62] G. Kresse and J. Furthmüller, Efficiency of ab-initio total energy calculations for metals and semiconductors using a plane-wave basis set, *Computational Materials Science* **6**, 15 (1996).
- [63] G. Kresse and J. Furthmüller, Software VASP, vienna (1999), *Physical Review B* **54**, 169 (1996).
- [64] D. Trots and S. Myagkota, High-temperature structural evolution of caesium and rubidium triiodoplumbates, *Journal of Physics and Chemistry of Solids* **69**, 2520 (2008).
- [65] A. Togo, First-principles Phonon Calculations with Phonopy and Phono3py, *Journal of the Physical Society of Japan* **92**, 012001 (2023).
- [66] A. Togo, L. Chaput, T. Tadano, and I. Tanaka, Implementation strategies in phonopy and phono3py, *Journal of Physics: Condensed Matter* **35**, 353001 (2023).
- [67] I. Souza, J. Íñiguez, and D. Vanderbilt, First-Principles Approach to Insulators in Finite Electric Fields, *Physical Review Letters* **89**, 117602 (2002).
- [68] Y. Su, K.-K. Song, M. Zhong, L.-B. Shi, and P. Qian, Stability and phonon-limited mobility for CsSnI<sub>3</sub> and CsPbI<sub>3</sub>, *Journal of Alloys and Compounds* **889**, 161723 (2021).
- [69] H.-Y. Gu, W.-J. Yin, and X.-G. Gong, Significant phonon anharmonicity drives phase transitions in CsPbI<sub>3</sub>, *Applied Physics Letters* **119**, 191101 (2021).

- [70] Y. Cao, G. Qi, C. Liu, L. Wang, Z. Ma, K. Wang, F. Du, G. Xiao, and B. Zou, Pressure-Tailored Band Gap Engineering and Structure Evolution of Cubic Cesium Lead Iodide Perovskite Nanocrystals, *The Journal of Physical Chemistry C* **122**, 9332 (2018).
- [71] G. D. Mahan, *Many Particle Physics*, 3rd ed., Physics of Solids and Liquids (Kluwer academic/Plenum pub, New York, 2000).
- [72] M. Schlipf, S. Ponc e, and F. Giustino, Carrier Lifetimes and Polaronic Mass Enhancement in the Hybrid Halide Perovskite CH<sub>3</sub>NH<sub>3</sub>PbI<sub>3</sub> from Multiphonon Fr ohlich Coupling, *Physical Review Letters* **121**, 086402 (2018).
- [73] J.-M. Lihm and S. Ponc e, Nonperturbative Self-Consistent Electron-Phonon Spectral Functions and Transport, *Physical Review Letters* **134**, 186401 (2025).
- [74] M. Houtput, <https://github.com/MHoutput/1e2ph-spectral/> (2026).

**Supplemental information for “Importance of nonlinear  
long-range electron-phonon interaction on the carrier mobility of  
anharmonic halide perovskites”**

Matthew Houtput,<sup>1</sup> Ingvar Zappacosta,<sup>1</sup> Serghei Klimin,<sup>1</sup>  
Samuel Poncé,<sup>2,3</sup> Jacques Tempere,<sup>1</sup> and Cesare Franchini<sup>4,5</sup>

<sup>1</sup>*Theory of Quantum Systems and Complex Systems,  
Universiteit Antwerpen, B-2000 Antwerpen, Belgium*

<sup>2</sup>*European Theoretical Spectroscopy Facility and Institute of Condensed  
Matter and Nanosciences, Université catholique de Louvain,  
Chemin des Étoiles 8, B-1348 Louvain-la-Neuve, Belgium*

<sup>3</sup>*WEL Research Institute, avenue Pasteur 6, 1300 Wavre, Belgium*

<sup>4</sup>*Faculty of Physics, Computational Materials Physics,  
University of Vienna, Kolingasse 14-16, Vienna A-1090, Austria*

<sup>5</sup>*Department of Physics and Astronomy,  
Alma Mater Studiorum - Università di Bologna, Bologna, 40127 Italy*

## S1. MOBILITY IN THE SERTA

In the main manuscript, we have described how to calculate the electron mobility in the SERTA using Eqs. (1)-(4). While these equations describe the physical intuition behind our method, they are not yet ready for a practical numerical evaluation. In this section, we provide the further analytical steps and approximations that lead to the expression for the mobility that we evaluate in practice. The chain of reasoning is very similar to the one presented in the supplementary information of [1].

We start from the following, general expression for the on-shell Fan-Migdal self energy in the diagonal band approximation, in terms of the two-argument Eliashberg function  $\alpha^2 F_{\mathbf{k},n}(\varepsilon, \omega)$  [2]:

$$\Sigma_{\mathbf{k}nn}^{\text{R}}(\varepsilon) = \hbar \int_{-\infty}^{+\infty} d\varepsilon' \int_0^{+\infty} d\omega \alpha^2 F_{\mathbf{k}nn}(\varepsilon', \omega) \left[ \frac{1 - f^0(\varepsilon') + n(\hbar\omega)}{\varepsilon - \varepsilon' - \hbar\omega + i\delta} + \frac{f^0(\varepsilon') + n(\hbar\omega)}{\varepsilon - \varepsilon' + \hbar\omega + i\delta} \right]. \quad (\text{S1})$$

Within the scope of this article, we are interested in the Eliashberg function calculated using only dipole long-range electron-phonon interaction. In [3], it is shown that the Eliashberg function in this case is given by the following expression:

$$\alpha^2 F_{\mathbf{k}nn}(\varepsilon', \omega) \approx \frac{e^2}{\varepsilon_0 (2\pi)^3} \int_{\mathbb{R}^3} d^3\mathbf{Q} \frac{\mathbf{Q} \cdot \mathcal{P}(\omega) \cdot \mathbf{Q}}{(\mathbf{Q} \cdot \boldsymbol{\varepsilon}^\infty \cdot \mathbf{Q})^2} \delta(\varepsilon' - \varepsilon_{\mathbf{k}+\mathbf{Q}n}), \quad (\text{S2})$$

Combining Eqs. (S1)-(S2), and evaluating the self energy on-shell by setting  $\varepsilon = \varepsilon_{\mathbf{k}n}$ , yields Eq. (4) from the main manuscript. We reproduce it here for clarity:

$$\begin{aligned} \Sigma_{\mathbf{k}nn}^{\text{R}}(\varepsilon_{\mathbf{k}n}) &= \frac{\hbar e^2}{\varepsilon_0 (2\pi)^3} \int_0^{+\infty} d\omega \int_{\mathbb{R}^3} d^3\mathbf{Q} \frac{\mathbf{Q} \cdot \mathcal{P}(\omega) \cdot \mathbf{Q}}{(\mathbf{Q} \cdot \boldsymbol{\varepsilon}^\infty \cdot \mathbf{Q})^2} \\ &\quad \times \left[ \frac{1 - f^0(\varepsilon_{\mathbf{k}+\mathbf{Q}n}) + n(\hbar\omega)}{\varepsilon_{\mathbf{k}n} - \varepsilon_{\mathbf{k}+\mathbf{Q}n} - \hbar\omega + i\delta} + \frac{f^0(\varepsilon_{\mathbf{k}+\mathbf{Q}n}) + n(\hbar\omega)}{\varepsilon_{\mathbf{k}n} - \varepsilon_{\mathbf{k}+\mathbf{Q}n} + \hbar\omega + i\delta} \right]. \quad (\text{S3}) \end{aligned}$$

For the rest of the derivation, we will limit ourselves to the case of cubic symmetry. In this case, both of the tensors  $\boldsymbol{\varepsilon}^\infty$  and  $\mathcal{P}(\omega)$  are reduced to scalars [3]:

$$\varepsilon_{\alpha\beta}^\infty = \varepsilon^\infty \delta_{\alpha\beta}, \quad (\text{S4})$$

$$\mathcal{P}_{\alpha\beta}(\omega) = \mathcal{P}(\omega) \delta_{\alpha\beta}. \quad (\text{S5})$$

With this assumption of cubic symmetry, Eq. (S3) for the on-shell retarded self energy

reduces to:

$$\begin{aligned} \Sigma_{\mathbf{k}nn}^{\text{R}}(\varepsilon_{\mathbf{k}n}) &= \frac{\hbar e^2}{\varepsilon_0(\varepsilon^\infty)^2(2\pi)^3} \int_0^{+\infty} d\omega \mathcal{P}(\omega) \int_{\mathbb{R}^3} \frac{d^3\mathbf{Q}}{|\mathbf{Q}|^2} \\ &\quad \times \left[ \frac{1 - f^0(\varepsilon_{\mathbf{k}+\mathbf{Q}n}) + n(\hbar\omega)}{\varepsilon_{\mathbf{k}n} - \varepsilon_{\mathbf{k}+\mathbf{Q}n} - \hbar\omega + i\delta} + \frac{f^0(\varepsilon_{\mathbf{k}+\mathbf{Q}n}) + n(\hbar\omega)}{\varepsilon_{\mathbf{k}n} - \varepsilon_{\mathbf{k}+\mathbf{Q}n} + \hbar\omega + i\delta} \right]. \end{aligned} \quad (\text{S6})$$

The theory of [3] then states that  $\mathcal{P}(\omega) = \mathcal{R}(\omega) + \mathcal{T}(\omega)$  is a dimensionless electron-phonon spectral function, which gets contributions from the one-electron-one-phonon and one-electron-two-phonon interactions.

We will now make two further assumptions. Firstly, we will assume that we are working with a single parabolic conduction band, given by:

$$\varepsilon_{\mathbf{k}} = \frac{\hbar^2|\mathbf{k}|^2}{2m^*}. \quad (\text{S7})$$

Here, without loss of generality, we adopt the convention that  $\mathbf{k} = \mathbf{0}$  lies at the minimum of the conduction band, even if that minimum does not occur at the  $\Gamma$ -point. We will drop the index  $n$  everywhere because we only have a single band. Secondly, we will assume that the band gap  $\Delta E$  of the material satisfies  $\exp(\Delta E/2k_B T) \gg 1$ . In this article, we focus on cubic CsPbI<sub>3</sub> which has a band gap of  $\Delta E = 1.7$  eV [4]. We also limit ourselves to temperatures below 500 K, which corresponds to  $k_B T = 0.043$  eV, so this approximation is excellent. In that case, we have  $n_F(\varepsilon_{\mathbf{k}}) \approx 0$ . Then, we get the following expression for the Fan-Migdal self energy:

$$\begin{aligned} \Sigma_{\mathbf{k}}^{\text{R}}(\varepsilon_{\mathbf{k}}) &= \lim_{\delta \rightarrow 0^+} -\frac{\hbar e^2}{\varepsilon_0(\varepsilon^\infty)^2(2\pi)^3} \int_0^{+\infty} d\omega \mathcal{P}(\omega) \\ &\quad \times \left( [1 + n_B(\omega)] \int_{\mathbb{R}^3} \frac{d^3\mathbf{Q}}{|\mathbf{Q}|^2} \frac{1}{\frac{\hbar^2|\mathbf{k}+\mathbf{Q}|^2}{2m^*} - \frac{\hbar^2|\mathbf{k}|^2}{2m^*} + \hbar\omega - i\delta} \right. \\ &\quad \left. + n_B(\omega) \int_{\mathbb{R}^3} \frac{d^3\mathbf{Q}}{|\mathbf{Q}|^2} \frac{1}{\frac{\hbar^2|\mathbf{k}+\mathbf{Q}|^2}{2m^*} - \frac{\hbar^2|\mathbf{k}|^2}{2m^*} - \hbar\omega - i\delta} \right). \end{aligned} \quad (\text{S8})$$

The remaining integrals over  $\mathbf{Q}$  can be calculated analytically. The general form of this integral also appears in the calculation of the quasiparticle energy of the Fröhlich polaron, so its result is known [5]:

$$\int_{\mathbb{R}^3} \frac{d^3\mathbf{Q}}{|\mathbf{Q}|^2} \frac{1}{\frac{\hbar^2|\mathbf{k}+\mathbf{Q}|^2}{2m^*} + C} = \frac{2\pi^2}{|\mathbf{k}|} \frac{2m^*}{\hbar^2} \arcsin \left( \sqrt{\frac{\frac{\hbar^2|\mathbf{k}|^2}{2m^*}}{\frac{\hbar^2|\mathbf{k}|^2}{2m^*} + C}} \right), \quad \text{where } C \in \mathbb{C} \setminus \mathbb{R}_0^-. \quad (\text{S9})$$

Therefore, the Fan-Migdal self energy is given by:

$$\begin{aligned} \Sigma_{\mathbf{k}}^{\text{R}}(\varepsilon_{\mathbf{k}}) &= \lim_{\delta \rightarrow 0^+} -\frac{e^2}{4\pi\varepsilon_0(\varepsilon^\infty)^2} \frac{2m^*}{\hbar|\mathbf{k}|} \int_0^{+\infty} d\omega \mathcal{P}(\omega) \\ &\times \left( [1 + n_B(\omega)] \arcsin \left( \sqrt{\frac{\hbar|\mathbf{k}|^2}{2m^*\omega}} \right) + n_B(\omega) \arcsin \left( \sqrt{\frac{\hbar|\mathbf{k}|^2}{-1 - i\delta}} \right) \right). \end{aligned} \quad (\text{S10})$$

To calculate the inverse lifetimes, we need to take the imaginary part of this expression.

Using the following identities, where  $a > 0$  and  $\Theta(a)$  is the Heaviside step function:

$$\text{Im} \left[ \lim_{\delta \rightarrow 0^+} \arcsin \left( \sqrt{\frac{a}{1 - i\delta}} \right) \right] = \text{arccosh}(\sqrt{a})\Theta(a - 1), \quad (\text{S11})$$

$$\text{Im} \left[ \lim_{\delta \rightarrow 0^+} \arcsin \left( \sqrt{\frac{a}{-1 - i\delta}} \right) \right] = \text{arcsinh}(\sqrt{a}), \quad (\text{S12})$$

we find the following expression for the inverse lifetimes:

$$\frac{1}{\tau_{\mathbf{k}}} = -2 \text{Im} [\Sigma_{\mathbf{k}}^{\text{R}}(\varepsilon_{\mathbf{k}})], \quad (\text{S13})$$

$$= \frac{2}{\hbar} \frac{e^2}{4\pi\varepsilon_0(\varepsilon^\infty)^2} \sqrt{\frac{2m^*}{\hbar}} \int_0^{+\infty} d\omega \frac{\mathcal{P}(\omega)}{\sqrt{\omega}} \varphi \left( \frac{\hbar^2|\mathbf{k}|^2}{2m^*k_{\text{B}}T}, \frac{\hbar\omega}{k_{\text{B}}T} \right). \quad (\text{S14})$$

Here, the auxiliary function  $\varphi(x, x_0)$  is defined as follows [1]:

$$\varphi(x, x_0) := \sqrt{\frac{x_0}{x}} \left( \frac{\text{arccosh} \left( \sqrt{\frac{x}{x_0}} \right) \Theta(x - x_0)}{1 - e^{-x_0}} + \frac{\text{arcsinh} \left( \sqrt{\frac{x}{x_0}} \right)}{e^{x_0} - 1} \right). \quad (\text{S15})$$

The scattering time  $\tau_{\mathbf{k}}$  is an isotropic function: it does not depend on the direction of  $\mathbf{k}$ . To highlight this, in [1] the inverse scattering times are written as  $\tau_{\mathbf{k}} = \tau \left( \frac{\hbar^2|\mathbf{k}|^2}{2m^*k_{\text{B}}T} \right)$ , where  $\tau(x)$  is given by:

$$\frac{1}{\tau(x)} = \frac{2}{\hbar} \frac{e^2}{4\pi\varepsilon_0(\varepsilon^\infty)^2} \sqrt{\frac{2m^*}{\hbar}} \int_0^{+\infty} d\omega \frac{\mathcal{P}(\omega)}{\sqrt{\omega}} \varphi \left( x, \frac{\hbar\omega}{k_{\text{B}}T} \right). \quad (\text{S16})$$

With the expression for the electron lifetimes known, the SERTA mobility can be evaluated using Eqs. (1)-(2) from the main part of the manuscript [1], given here for a single conduction band:

$$\mu_{\alpha\beta} \approx -\frac{e}{n_e(2\pi)^3} \int_{\text{1BZ}} d^3\mathbf{k} \frac{\partial f^0(\varepsilon_{\mathbf{k}})}{\partial \varepsilon_{\mathbf{k}}} v_{\mathbf{k}\alpha} v_{\mathbf{k}\beta} \tau_{\mathbf{k}}. \quad (\text{S17})$$

We require two more elements in this expression: the band velocities  $v_{\mathbf{k}\alpha}$ , and the quantity  $\frac{1}{n_e} \frac{\partial f^0(\varepsilon_{\mathbf{k}})}{\partial \varepsilon_{\mathbf{k}}}$ . For a parabolic band given by Eq. (S7), the band velocities are easily calculated

from the definition:

$$\begin{aligned} v_{\mathbf{k}\alpha} &= \frac{1}{\hbar} \frac{\partial \varepsilon_{\mathbf{k}}}{\partial k_{\alpha}}, \\ &= \frac{\hbar k_{\alpha}}{m^*} \end{aligned} \quad (\text{S18})$$

For the quantity  $\frac{1}{n_e} \frac{\partial f^0(\varepsilon_{\mathbf{k}})}{\partial \varepsilon_{\mathbf{k}}}$  we will once again assume that  $\Delta E \gg 2k_{\text{B}}T$ , so the Fermi-Dirac distribution is well approximated by a Boltzmann distribution:

$$f^0(\varepsilon) \approx \exp\left(\frac{\mu}{k_{\text{B}}T}\right) \exp\left(-\frac{\varepsilon}{k_{\text{B}}T}\right), \quad (\text{S19})$$

$$\Rightarrow \frac{\partial f^0(\varepsilon)}{\partial \varepsilon} \approx -\frac{1}{k_{\text{B}}T} \exp\left(\frac{\mu}{k_{\text{B}}T}\right) \exp\left(-\frac{\hbar^2|\mathbf{k}|^2}{2m^*k_{\text{B}}T}\right). \quad (\text{S20})$$

We may also calculate the electron density under this approximation: The electron density becomes:

$$n_e = \frac{1}{(2\pi)^3} \int_{\text{1BZ}} d^3\mathbf{k} f^0(\varepsilon_{\mathbf{k}}), \quad (\text{S21})$$

$$\approx \exp\left(\frac{\mu}{k_{\text{B}}T}\right) \frac{1}{(2\pi)^3} \int_{\mathbb{R}^3} d^3\mathbf{k} \exp\left(-\frac{\hbar^2|\mathbf{k}|^2}{2m^*k_{\text{B}}T}\right), \quad (\text{S22})$$

$$= \exp\left(\frac{\mu}{k_{\text{B}}T}\right) \frac{1}{8\pi^{\frac{3}{2}}} \left(\frac{2m^*k_{\text{B}}T}{\hbar^2}\right)^{\frac{3}{2}}. \quad (\text{S23})$$

To go from the first to the second line, we assumed that the integral is converged before  $|\mathbf{k}|$  reaches the edge of the first Brillouin zone, so the integration domain can be approximately replaced by  $\mathbb{R}^3$ . We find that  $\frac{1}{n_e} \frac{\partial f^0(\varepsilon_{\mathbf{k}})}{\partial \varepsilon_{\mathbf{k}}}$  is independent of the chemical potential. Plugging this back into Eq. (S17) for the electron mobility yields:

$$\mu_{\alpha\beta} \approx \frac{e}{m^*} \frac{2}{\pi^{\frac{3}{2}}} \left(\frac{\hbar^2}{2m^*k_{\text{B}}T}\right)^{\frac{5}{2}} \int_{\mathbb{R}^3} d^3\mathbf{k} k_{\alpha} k_{\beta} \exp\left(-\frac{\hbar^2|\mathbf{k}|^2}{2m^*k_{\text{B}}T}\right) \tau\left(\frac{\hbar^2|\mathbf{k}|^2}{2m^*k_{\text{B}}T}\right). \quad (\text{S24})$$

This integral is most easily evaluated in spherical coordinates,  $\mathbf{k} = k\mathbf{n}$  where  $k \in [0, +\infty[$  and  $\mathbf{n} \in S^2$  is a direction vector on the unit sphere. Then, the integral factorizes in a radial and angular part:

$$\mu_{\alpha\beta} \approx \frac{e}{m^*} \frac{2}{\pi^{\frac{3}{2}}} \left(\frac{\hbar^2}{2m^*k_{\text{B}}T}\right)^{\frac{5}{2}} \int_{S^2} d^2\mathbf{n} n_{\alpha} n_{\beta} \int_0^{+\infty} dk k^4 \exp\left(-\frac{\hbar^2 k^2}{2m^*k_{\text{B}}T}\right) \tau\left(\frac{\hbar^2 k^2}{2m^*k_{\text{B}}T}\right). \quad (\text{S25})$$

The angular integral can be calculated explicitly. From symmetry it can be seen that it is zero when  $\alpha \neq \beta$ , and that result does not depend on the value of  $\alpha$  when  $\alpha = \beta$ . Therefore,

we only need to calculate the case  $\alpha = \beta = z$ :

$$\int_{S^2} d^2\mathbf{n} n_\alpha n_\beta = \int_{S^2} d^2\mathbf{n} n_z^2 \delta_{\alpha\beta}, \quad (\text{S26})$$

$$= \int_0^\pi d\theta \int_0^{2\pi} d\phi \cos^2(\theta) \sin(\theta) \delta_{\alpha\beta}, \quad (\text{S27})$$

$$= \frac{4\pi}{3} \delta_{\alpha\beta} \quad (\text{S28})$$

This means the mobility tensor can be written as  $\mu_{\alpha\beta} = \mu\delta_{\alpha\beta}$ : it is isotropic, as expected for a cubic material. The isotropic mobility is given by:

$$\mu \approx \frac{e}{m^*} \frac{8}{3\sqrt{\pi}} \left( \frac{\hbar^2}{2m^*k_B T} \right)^{\frac{5}{2}} \int_0^{+\infty} dk k^4 \exp\left(-\frac{\hbar^2 k^2}{2m^*k_B T}\right) \tau\left(\frac{\hbar^2 k^2}{2m^*k_B T}\right). \quad (\text{S29})$$

Finally, we make the substitution  $x := \frac{\hbar^2 k^2}{2m^*k_B T}$  to arrive at our practical expression for the SERTA:

$$\mu = \frac{e}{m^*} \left[ \frac{4}{3\sqrt{\pi}} \int_0^{+\infty} dx \tau(x) x^{\frac{3}{2}} e^{-x} \right]. \quad (\text{S30})$$

To evaluate  $\tau(x)$  in practice, we use expression Eq. (S16), where we use  $\mathcal{P}(\omega) = \mathcal{R}(\omega) + \mathcal{T}(\omega)$  as defined by Eq. (5) and Eqs. (10)-(11):

$$\begin{aligned} \frac{1}{\tau(x)} = \frac{1}{\hbar\Omega_0} \frac{e^4}{4\pi\varepsilon_0^2(\varepsilon^\infty)^2} \sqrt{\frac{2m^*}{\hbar}} \sum_{\nu \in \text{LO}} \frac{|p_\nu|^2}{\omega_\nu^{\frac{3}{2}}} \varphi\left(x, \frac{\hbar\omega_\nu}{k_B T}\right) \\ + \frac{2}{\hbar} \frac{e^2}{4\pi\varepsilon_0(\varepsilon^\infty)^2} \sqrt{\frac{2m^*}{\hbar}} \int_0^{+\infty} d\omega \frac{\mathcal{T}(\omega)}{\sqrt{\omega}} \varphi\left(x, \frac{\hbar\omega}{k_B T}\right), \end{aligned} \quad (\text{S31})$$

where we recall that  $\varphi(x, x_0)$  is simply the analytical function given in Eq. (S15). For a given temperature and electron-phonon spectral function  $\mathcal{T}(\omega)$ , expression Eq. (S31) is evaluated through numerical integration. The result is used in Eq. (S30) to calculate the mobility through one more numerical integration.

## S2. DFT INPUT PARAMETERS

### A. Electronic parameters

Our calculations are performed in VASP [6, 7] with the Perdew-Burke-Ernzerhof (PBE) functional. We choose  $a = 6.276$  Å for the lattice parameter as in [1], which is close to the experimental lattice parameter of  $a = 6.289$  Å [8]. For our pseudopotentials, we choose GW pseudopotentials from the VASP potpaw.64 dataset, in order to have access to

pseudopotentials that contain the  $5s^2$  and  $5p^6$  states for lead. Specifically, we choose the following pseudopotentials: Cs\_sv\_GW [ $5s^2$   $5p^6$   $6s^1$ ] for cesium, Pb\_sv\_GW [ $5s^2$   $5p^6$   $5d^{10}$   $6s^2$   $6p^2$ ] for lead, and I\_GW [ $5s^2$   $5p^5$ ] for iodine. The plane wave cutoff energy was set to 600 eV. Unit cell properties are calculated on a  $\mathbf{k}$ -grid of size  $8 \times 8 \times 8$ . For phonon properties calculated on a  $2 \times 2 \times 2$  supercell, an appropriately scaled  $\mathbf{k}$ -grid of size  $4 \times 4 \times 4$  is used. The Born effective charge tensor  $\mathbf{Z}_\kappa$  and dielectric tensor  $\epsilon^\infty$  are calculated from density functional perturbation theory (DFPT) with a  $16 \times 16 \times 16$   $\mathbf{k}$ -grid. All results in the manuscript are calculated without spin-orbit coupling.

## B. Phonon parameters

As in [3], the phonon properties are calculated using the finite displacement method implemented in the PhonoPy package [9, 10]. The phonon frequencies must be converged with respect to the supercell size, and the magnitude  $\Delta x$  of the ion displacements. We found that the phonon frequencies are more or less converged after choosing  $\Delta x = 0.005$  Å: more motivation for this value is provided later in this section. We will show in a moment that the calculations for the nonlinear electron-phonon interaction require strict convergence tolerances, making the calculations computationally expensive. Therefore, we are limited to small supercells, and as such, all phonon results in this manuscript are computed on a  $2 \times 2 \times 2$  supercell.

## C. Parameters for $\mathcal{T}(\omega)$

The evaluation of the one-electron-two-phonon spectral function  $\mathcal{T}(\omega)$  through Eq. (5) requires an integral over Dirac delta functions over the first Brillouin zone. As in [3], we calculate these integrals using the smearing method. We replace the Dirac delta with a Gaussian with a finite width  $\sigma = 0.025$  THz:

$$\delta(\omega) \rightarrow \frac{1}{\sqrt{2\pi\sigma}} e^{-\frac{\omega^2}{2\sigma^2}} \quad (\text{S32})$$

Then, the integral over the first Brillouin zone is evaluated using the trapezoid rule on a fine  $\mathbf{q}$ -grid. All quantities are interpolated from the coarse  $2 \times 2 \times 2$  commensurate grid to the fine grid by Fourier interpolation [3]. We use a  $128 \times 128 \times 128$  fine  $\mathbf{q}$ -grid for all results

of the electron-phonon spectral function, and a  $32 \times 32 \times 32$  fine  $\mathbf{q}$ -grid for all results of the electron lifetime and mobility.

For the calculation of the electric field derivative of the dynamical matrix  $\frac{\partial \mathcal{D}_{\kappa\alpha, \kappa'\beta}(\mathbf{q})}{\partial \mathcal{E}_z}$  that appears in Eqs. (8)-(9) of the main manuscript, there are several numerical parameters which we must pay special attention to. We again follow [3], where the derivative of the dynamical matrix is approximated by a finite difference:

$$\frac{\partial \mathcal{D}_{\kappa\alpha, \kappa'\beta}(\mathbf{q})}{\partial \mathcal{E}_z} \approx \frac{\mathcal{D}_{\kappa\alpha, \kappa'\beta}(\mathbf{q}, \mathcal{E}_z) - \mathcal{D}_{\kappa\alpha, \kappa'\beta}(\mathbf{q}, -\mathcal{E}_z)}{2\mathcal{E}_z} + O(\mathcal{E}_z^3) \quad (\text{S33})$$

We need to calculate the dynamical matrix from first principles, using a calculation with an appropriate value of the external electric field  $\mathcal{E}_z$ . The main issue in practice is if we choose  $\mathcal{E}_z$  too small, the change in the dynamical matrix may be smaller than the numerical noise that is introduced during the calculation. Therefore, we should choose  $\mathcal{E}_z$  as large as possible. Additionally, we need to set the convergence tolerance  $E_{\text{tol}}$  of the self-consistent electronic loop (the EDIFF flag in VASP) to a value that is strict enough, to ensure that the resulting dynamical matrix is precise enough to see the effect of the electric field.

The electric field strength  $\mathcal{E}_z$  must be chosen well below the onset of Zener breakdown, where the electric enthalpy function loses its minima [11]. This occurs when:

$$E_z^{(\text{Zener})} = \frac{\Delta E}{eaN_{\mathbf{k}}} = 0.033 \frac{\text{V}}{\text{\AA}} \quad (\text{S34})$$

Here,  $N_{\mathbf{k}} = 8$  is the number of  $\mathbf{k}$ -points in the  $z$ -direction. To satisfy this criterion, we choose  $\mathcal{E}_z = 0.0025 \frac{\text{V}}{\text{\AA}}$  for the calculation of the electric field derivative of the dynamical matrix.

To choose an appropriate value for the convergence tolerance of the self-consistent electronic loop, we introduce a quantitative measure of the numerical error introduced during the first principles calculations. In [3], it was shown that in the cubic perovskite structure, these two dynamical matrices are actually related by a complex conjugate:

$$\mathcal{D}_{\kappa\alpha, \kappa'\beta}(\mathbf{q}, -\mathcal{E}_z) = \mathcal{D}_{\kappa\alpha, \kappa'\beta}(\mathbf{q}, \mathcal{E}_z)^*. \quad (\text{S35})$$

From this property, it follows that for a perfect calculation:

$$\text{Im} [\mathcal{D}_{\kappa\alpha, \kappa'\beta}(\mathbf{q}_c, \mathcal{E}_z)] + \text{Im} [\mathcal{D}_{\kappa\alpha, \kappa'\beta}(\mathbf{q}_c, -\mathcal{E}_z)] = 0. \quad (\text{S36})$$

However, in practice, the dynamical matrix at  $+\mathcal{E}_z$  and  $-\mathcal{E}_z$  are calculated independently, and the above property is not exactly satisfied. If the result is far from zero, this is an

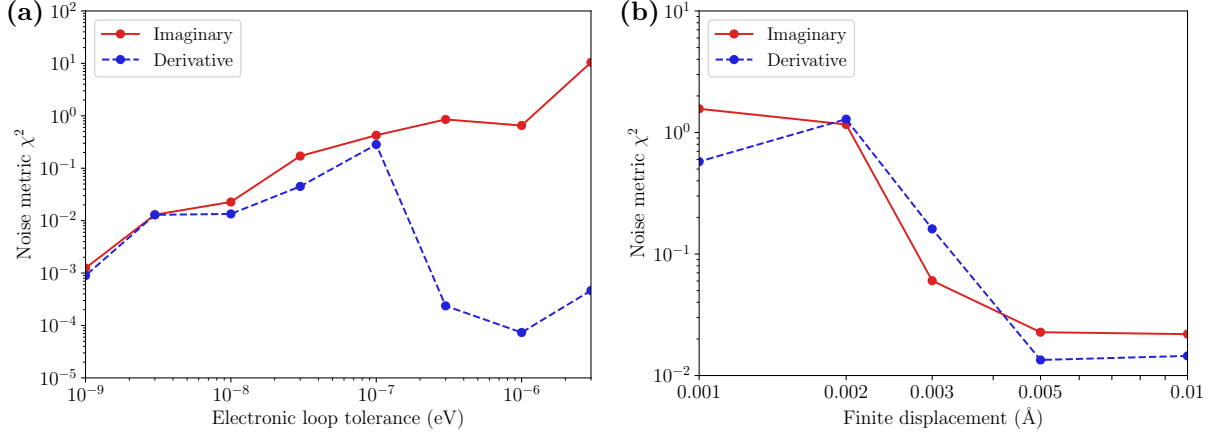


Figure S1. Noise metrics  $\chi_{\text{imag}}^2$  and  $\chi_{\text{der}}^2$ : **(a)** as a function of the convergence tolerance  $E_{\text{tol}}$  of the self-consistent electronic loop, calculated with  $\Delta x = 0.005 \text{ \AA}$ ; **(b)** as a function of the finite displacement  $\Delta x$  used to calculate the phonon properties, calculated with  $E_{\text{tol}} = 10^{-8} \text{ eV}$ . The noise metrics are small enough once  $E_{\text{tol}} \lesssim 10^{-8} \text{ eV}$  and  $\Delta x \gtrsim 0.005 \text{ \AA}$ .

indication of a significant numerical error in the calculation. We can turn this intuition into a single number by summing over all  $\kappa\alpha, \kappa'\beta$ , and all commensurate points  $\mathbf{q}_c \neq \mathbf{0}$ . We exclude the  $\Gamma$ -point explicitly because  $\text{Im}[\mathcal{D}_{\kappa\alpha, \kappa'\beta}(\mathbf{0}, \mathcal{E}_z)] = 0$ . We introduce the following “noise metric”  $\chi_{\text{imag}}^2$ , which is a dimensionless number:

$$\chi_{\text{imag}}^2 := \frac{\sum_{\mathbf{q}_c \neq \mathbf{0}} \sum_{\kappa\alpha} \sum_{\kappa'\beta} \left( \text{Im}[\mathcal{D}_{\kappa\alpha, \kappa'\beta}(\mathbf{q}_c, \mathcal{E}_z)] + \text{Im}[\mathcal{D}_{\kappa\alpha, \kappa'\beta}(\mathbf{q}_c, -\mathcal{E}_z)] \right)^2}{\max_{\mathbf{q}_c \neq \mathbf{0}} \max_{\kappa\alpha} \max_{\kappa'\beta} \left( \text{Im}[\mathcal{D}_{\kappa\alpha, \kappa'\beta}(\mathbf{q}_c, \mathcal{E}_z)] - \text{Im}[\mathcal{D}_{\kappa\alpha, \kappa'\beta}(\mathbf{q}_c, -\mathcal{E}_z)] \right)^2} \quad (\text{S37})$$

We also introduce a similar metric  $\chi_{\text{der}}^2$ , based on the fact that the derivative of the dynamical matrix should be purely imaginary in the cubic perovskite structure:

$$\chi_{\text{der}}^2 := \frac{\sum_{\mathbf{q}_c \neq \mathbf{0}} \sum_{\kappa\alpha} \sum_{\kappa'\beta} \text{Re} \left[ \frac{\partial \mathcal{D}_{\kappa\alpha, \kappa'\beta}(\mathbf{q}_c)}{\partial \mathcal{E}_z} \right]^2}{\max_{\mathbf{q}_c \neq \mathbf{0}} \max_{\kappa\alpha} \max_{\kappa'\beta} \left| \frac{\partial \mathcal{D}_{\kappa\alpha, \kappa'\beta}(\mathbf{q}_c)}{\partial \mathcal{E}_z} \right|^2} \quad (\text{S38})$$

where  $\frac{\partial \mathcal{D}_{\kappa\alpha, \kappa'\beta}(\mathbf{q})}{\partial \mathcal{E}_z}$  is calculated using Eq. (S33). Both  $\chi_{\text{imag}}^2$  and  $\chi_{\text{der}}^2$  can be interpreted as follows. If  $\chi_{\text{imag}}^2$  (resp.  $\chi_{\text{der}}^2$ ) is close to zero, the calculation of the imaginary part (resp. the derivative) of the dynamical matrix is accurate; the larger  $\chi^2$ , the more numerical noise is

present in the calculations. If  $\chi^2 \approx 1$ , we can very roughly estimate that the numerical noise is around the same order of magnitude of the values of the actual elements we are trying to calculate. This is obviously something to be avoided, so we should aim for a value of  $\chi^2 \ll 1$ .

In practice, we only use the imaginary part of the dynamical matrix to calculate  $\frac{\partial \mathcal{D}_{\kappa\alpha,\kappa'\beta}(\mathbf{q})}{\partial \mathcal{E}_z}$  [3]. Indeed, from Eq. (S35), it can be shown that only the imaginary part contributes to Eq. (S33). Therefore,  $\chi_{\text{imag}}^2$  is the most important metric of the two. We use  $\chi_{\text{der}}^2$  as a consistency check. Indeed, the derivative of the dynamical matrix should be equal to the imaginary part of the dynamical matrix, up to a constant prefactor [3]. Therefore, if the calculation is accurate, we also expect  $\chi_{\text{imag}}^2 \approx \chi_{\text{der}}^2$ .

Having introduced the noise metrics  $\chi_{\text{imag}}^2$  and  $\chi_{\text{der}}^2$ , we may now calculate the dynamical matrix at  $\mathcal{E}_z = \pm 0.0025$  Å for various values of the ionic displacement magnitude  $\Delta x$  and the convergence tolerance  $E_{\text{tol}}$  of the self-consistent electronic loop. Fig. S1 shows the noise metrics  $\chi_{\text{imag}}^2$  and  $\chi_{\text{der}}^2$  as a function of these two numerical parameters. For phonon calculations using the VASP + PhonoPy workflow, it is usually recommended to set  $E_{\text{tol}} = 10^{-6}$  eV. However, from Fig. S1a it is clear that the results for the electric field calculations will not be reliable with this value, since  $\chi_{\text{imag}}^2 \approx 1$  and  $\chi_{\text{imag}}^2 \neq \chi_{\text{der}}^2$ . Instead, we should choose a lower value of  $E_{\text{tol}}$ , keeping in mind that lower values mean longer computation times. For all calculations in the main part of the manuscript, we choose the value  $E_{\text{tol}} = 10^{-8}$  eV as a good compromise. For clarity, we note that the dynamical matrix  $\mathcal{D}_{\kappa\alpha,\kappa'\beta}(\mathbf{q})$  and derived phonon properties will be accurately calculated even at  $E_{\text{tol}} = 10^{-6}$  eV; it is only for an accurate calculation of the derivative  $\frac{\partial \mathcal{D}_{\kappa\alpha,\kappa'\beta}(\mathbf{q})}{\partial \mathcal{E}_z}$  that we need a stricter value. Similarly, from Fig. S1b we may conclude that the results for the derivative of the dynamical matrix are reliable for  $\Delta x = 0.005$  Å, which is the value that we choose for all calculations in this manuscript. Although we would find even more accurate phonon frequencies by choosing  $\Delta x$  even lower, reliable results for  $\frac{\partial \mathcal{D}_{\kappa\alpha,\kappa'\beta}(\mathbf{q}_c)}{\partial \mathcal{E}_z}$  would require even lower values of  $E_{\text{tol}}$  in this case.

To verify that the physically relevant results are converged with our choice of  $E_{\text{tol}}$ , we calculated the one-electron-two-phonon spectral function  $\mathcal{T}(\omega)$  for several values of this numerical parameter. Fig. S2 shows that  $\mathcal{T}(\omega)$  is indeed converged when it is calculated using  $E_{\text{tol}} = 10^{-8}$  eV, since the result is essentially the same as the result calculated using  $E_{\text{tol}} = 10^{-9}$  eV. It can also be seen that using the usual value  $E_{\text{tol}} = 10^{-6}$  eV results in a

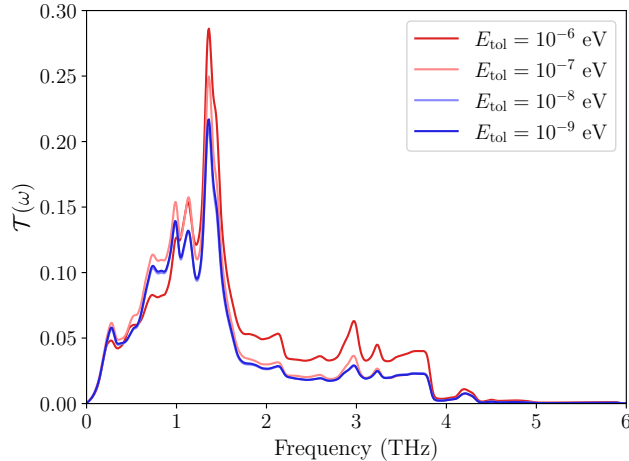


Figure S2. Convergence of the one-electron-two-phonon spectral function  $\mathcal{T}(\omega)$  with respect to the convergence tolerance  $E_{\text{tol}}$  of the self-consistent electronic loop.

one-electron-two-phonon spectral function that is too large, especially at higher frequencies.

- 
- [1] S. Ponc e, M. Schlipf, and F. Giustino, Origin of Low Carrier Mobilities in Halide Perovskites, [ACS Energy Letters](#) **4**, 456 (2019).
  - [2] F. Giustino, Electron-phonon interactions from first principles, [Reviews of Modern Physics](#) **89**, 015003 (2017).
  - [3] M. Houtput, L. Ranalli, C. Verdi, S. Klimin, S. Ragni, C. Franchini, and J. Tempere, First-principles theory of nonlinear long-range electron-phonon interaction, [Physical Review B](#) **111**, 184320 (2025).
  - [4] Y. Cao, G. Qi, C. Liu, L. Wang, Z. Ma, K. Wang, F. Du, G. Xiao, and B. Zou, Pressure-Tailored Band Gap Engineering and Structure Evolution of Cubic Cesium Lead Iodide Perovskite Nanocrystals, [The Journal of Physical Chemistry C](#) **122**, 9332 (2018).
  - [5] G. D. Mahan, *Many Particle Physics*, 3rd ed., Physics of Solids and Liquids (Kluwer academic/Plenum pub, New York, 2000).
  - [6] G. Kresse and J. Furthm uller, Efficiency of ab-initio total energy calculations for metals and semiconductors using a plane-wave basis set, [Computational Materials Science](#) **6**, 15 (1996).
  - [7] G. Kresse and J. Furthm uller, Software VASP, vienna (1999), [Physical Review B](#) **54**, 169 (1996).

- [8] D. Trots and S. Myagkota, High-temperature structural evolution of caesium and rubidium triiodoplumbates, [Journal of Physics and Chemistry of Solids](#) **69**, 2520 (2008).
- [9] A. Togo, First-principles Phonon Calculations with Phonopy and Phono3py, [Journal of the Physical Society of Japan](#) **92**, 012001 (2023).
- [10] A. Togo, L. Chaput, T. Tadano, and I. Tanaka, Implementation strategies in phonopy and phono3py, [Journal of Physics: Condensed Matter](#) **35**, 353001 (2023).
- [11] I. Souza, J. Íñiguez, and D. Vanderbilt, First-Principles Approach to Insulators in Finite Electric Fields, [Physical Review Letters](#) **89**, 117602 (2002).